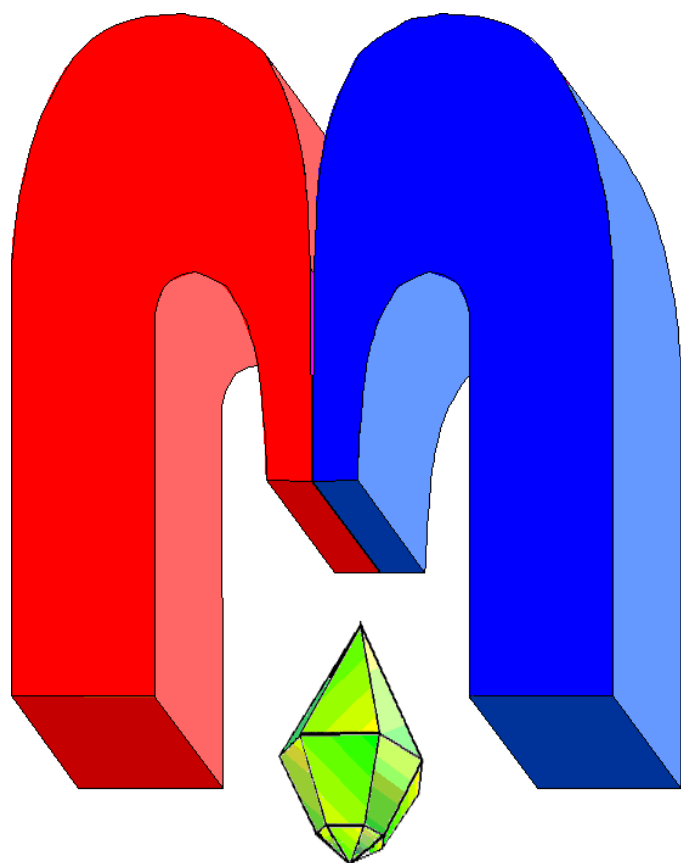


ISSN 2072-5981

doi: 10.26907/mrsej



***Magnetic
Resonance
in Solids***

Electronic Journal

Volume 27

Issue 1

Article No 25101

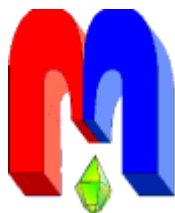
1-14 pages

2025

doi: [10.26907/mrsej-25101](https://doi.org/10.26907/mrsej-25101)

<http://mrsej.kpfu.ru>

<http://mrsej.elpub.ru>



Established and published by Kazan University*
Endorsed by International Society of Magnetic Resonance (ISMAR)
Registered by Russian Federation Committee on Press (#015140),
August 2, 1996
First Issue appeared on July 25, 1997

© Kazan Federal University (KFU)†

"Magnetic Resonance in Solids. Electronic Journal" (MRSej) is a peer-reviewed, all electronic journal, publishing articles which meet the highest standards of scientific quality in the field of basic research of a magnetic resonance in solids and related phenomena.

Indexed and abstracted by
Web of Science (ESCI, Clarivate Analytics, from 2015), Scopus (Elsevier, from 2012), RusIndexSC (eLibrary, from 2006), Google Scholar, DOAJ, ROAD, CyberLeninka (from 2006), SCImago Journal & Country Rank, etc.

Editor-in-Chief

Boris **Kochelaev** (KFU, Kazan)

Honorary Editors

Jean **Jeener** (Universite Libre de Bruxelles, Brussels)


Raymond **Orbach** (University of California, Riverside)

Executive Editor

Yurii **Proshin** (KFU, Kazan)
mrsej@kpfu.ru



This work is licensed under a [Creative Commons Attribution-ShareAlike 4.0 International License](https://creativecommons.org/licenses/by-sa/4.0/).

 This is an open access journal which means that all content is freely available without charge to the user or his/her institution. This is in accordance with the [BOAI definition of open access](https://www.boai.gov.ru/).

Technical Editor

Maxim **Avdeev** (KFU, Kazan)

Editors

Vadim **Atsarkin** (Institute of Radio Engineering and Electronics, Moscow)

Yurij **Bunkov** (CNRS, Grenoble)

Mikhail **Eremin** (KFU, Kazan)

David **Fushman** (University of Maryland, College Park)

Hugo **Keller** (University of Zürich, Zürich)

Yoshio **Kitaoka** (Osaka University, Osaka)

Boris **Malkin** (KFU, Kazan)

Alexander **Shengelaya** (Tbilisi State University, Tbilisi)

Jörg **Sichelschmidt** (Max Planck Institute for Chemical Physics of Solids, Dresden)

Haruhiko **Suzuki** (Kanazawa University, Kanazawa)

Murat **Tagirov** (KFU, Kazan)

Dmitrii **Tayurskii** (KFU, Kazan)

Valentine **Zhikharev** (KNRTU, Kazan)

* Address: "Magnetic Resonance in Solids. Electronic Journal", Kazan Federal University; Kremlevskaya str., 18; Kazan 420008, Russia

† In Kazan University the Electron Paramagnetic Resonance (EPR) was discovered by Zavoisky E.K. in 1944.

DFT study of magnetic order in Fe-Al-based ternary alloys

A.F. Abdullin*, E.V. Voronina

Kazan Federal University, Kazan 420008, Russia

**E-mail: ayazik@bk.ru*

(Received November 1, 2024; revised December 21, 2024;
accepted December 28, 2024; published January 9, 2025)

In this study, we utilized quantum-mechanical calculations to explore the electronic structure of binary and ternary Fe-Al-based systems with noncollinear magnetic configurations. Our findings indicate that the ground state of systems, such as Fe_9Al_7 , $\text{Fe}_9\text{Al}_6\text{B}$, $\text{Fe}_9\text{Al}_6\text{Ga}$, and Fe_9Ga_6 , is not ferromagnetic, but rather exhibits a spin spiral structure in the [111] direction. We analyzed the effects of different types of exchange-correlation potentials, aluminum concentration, relaxation of interatomic distances, substituting atom positions, and spin wave orientations on magnetic properties. Various exchange-correlation potentials consistently demonstrated the dependency of the total energy on the spin spiral q -vector, with the generalized gradient approximation closely matching experimental observations. In the Fe_9Al_7 unit cell, a spin spiral structure prevails at 43.75% atomic Al, while other compositions favor ferromagnetism. The system can support spin spiral vectors in the [001], [110], and [111] directions, with [111] being the most energetically favorable. The equilibrium state is highly sensitive to the position and type of sp -elements within the unit cell. Overall, our results show that spin spiral structures with the [111] q -vector are energetically favored when the average magnetic moment is approximately $1 \mu_B$ per Fe atom, which is consistent with Mössbauer data.

PACS: 71.15.Mb, 75.10.-b, 75.30.Ds, 75.50.Bb.

Keywords: DFT, Fe-Al, Fe-Al-B, Fe-Al-Ga, noncollinear magnetism, ternary alloys, nuclear resonance, SDW, spin spiral wave

1. Introduction

The magnetic state of binary Fe-Al and Fe-Al-based multicomponent alloys remains a subject of significant scientific and practical interest today. Particularly intriguing is the task of determining the type of magnetic ordering in iron aluminides with a cubic structure and aluminum content above 25 atomic percent. The unusual magnetic behavior of these ordered systems was explained by antiferromagnetic indirect exchange [1, 2], cluster magnetism [3], and variants of spin glass states (micromagnetism and reentrant spin glass) [4–6].

In ordered Fe-Al alloys with aluminum concentrations ranging from 34 to 43 atomic percent at 1.7 K, neutron diffraction methods revealed correlations of the magnetic moment associated with incommensurate spin density waves (ISDW) [7, 8]. Theoretical studies of the electronic structure and magnetic state of the equilibrium intermetallic compound FeAl near stoichiometry [9, 10] have shown that this system is characterized by several magnetic states with very close energies (< 1 mRy). First-principles calculations predicted that in the Fe_9Al_7 system, the formation of a spin spiral magnetic state is possible with very low stabilization energy (0.1 mRy below the ferromagnetic state). Comprehensive studies of the high-aluminum compound FeAl_2 [11] provided direct evidence of incommensurate magnetic ordering of antiferromagnetically coupled Fe magnetic moments.

Long-period incommensurate noncollinear (and collinear) magnetic structures, in which the magnetic moments of atoms are oriented at specific angles relative to each other and the amplitude of the magnetic moment periodically varies from site to site, can significantly influence the magnetic and electronic properties of the material. Aluminum and gallium are isoelectronic

elements, leading to similar magnetic properties in Fe-Al and Fe-Ga systems. The compound Fe_3Ga_4 exhibits a cascade of magnetic transitions [12, 13] from a ferromagnetic ground state to the ISDW at intermediate temperatures (68–360 K), and then from ISDW through a return to ferromagnetism to a paramagnetic state at high temperatures. As noted by the authors of this study, the sequence of transitions, driven by the incommensurate ISDW due to the nesting of the Fermi surface [13], allows for potential applications in magnetic memory devices and spintronics. The presence of these magnetic structures leads to complex interactions that significantly affect the macroscopic properties of the materials, including magnetic anisotropy, domain structure, and magnetoresistance.

Modern computational methods, including those based on Density Functional Theory (DFT), have become indispensable tools for investigating the electronic and magnetic properties of materials. For example, theoretical studies of Fe systems with *sp*-elements [14–16] have revealed essential information about exchange interactions and magnetic coupling mechanisms that govern the magnetic ordering in these alloys, emphasizing the complex interplay between structural and electronic factors.

Adding a third element (M) to Fe-Al alloys provides additional opportunities to control their magnetic properties. In ternary Fe-Al-M alloys, the composition and concentration of the third element can significantly influence both the crystal structure and the type of magnetic ordering. Magnetic phase transitions in these compounds are of particular interest. Depending on the type and concentration of the third component, such as boron (B) or gallium (Ga), magnetic interactions can be substantially altered, leading to the stabilization of new magnetic phases or the modification of existing ones. For instance, in Fe-Al-B and Fe-Al-Ga alloys, the addition of boron or gallium modifies local interatomic distances, the *bcc* lattice parameter [17, 18], and the local atomic and magnetic environment. These modifications affect the temperature of magnetic transitions and influence the stability of long-period incommensurate noncollinear (and collinear) magnetic structures. Integrating theoretical studies with experimental data is crucial for understanding the influence of the third component on the electronic structure and magnetic properties of alloys, ultimately guiding the development of advanced materials for technological applications.

Despite experimental studies supporting the realization of ISDW in ternary Fe-Al-M systems [19, 20], the detailed mechanism underlying the destruction of ferromagnetic order and the transition to the ISDW state remains incompletely understood. This gap in understanding necessitates further theoretical investigation using advanced computational methods, such as DFT, which can provide insights into the roles of electronic structure, lattice distortions, and atomic substitutions in these phase transitions. Moreover, from a practical standpoint, the ability to control the magnetic state of ternary Fe-Al-based alloys through materials engineering opens new possibilities for designing materials with desired magnetic characteristics. This has significant implications for the development of advanced magnetic materials for various technological applications, such as magnetic sensors and components of spintronic devices.

In this study, we use DFT calculations to investigate the magnetic properties of the binary Fe-Al system and its ternary derivatives. Our focus will be on the spin spiral structures to understand how various parameters influence their energetic stability.

2. Calculation methods

The supercell consisting of 16 atoms – Fe_9Al_7 (Figure 1) – was chosen as the reference unit cell. Quantum-mechanical calculations were performed using the WIENncm program [21], which ex-

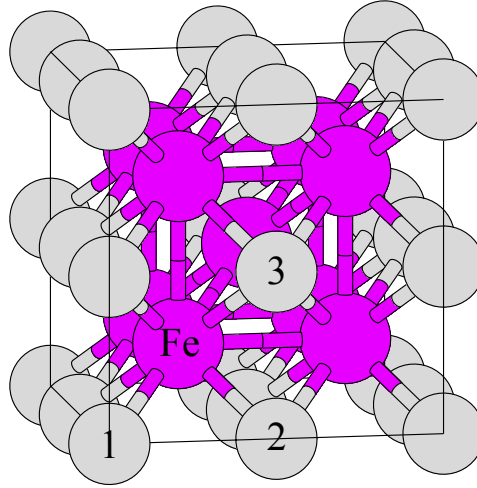


Figure 1. Unit cell of Fe_9Al_7 . Purple spheres represent iron atoms, and gray spheres represent aluminum atoms. The numbers 1, 2, and 3 indicate the nonequivalent positions of aluminum atoms, with coordinates $(0;0;0)$, $(0;0;1/2)$, and $(1/2;1/2;0)$, respectively.

tends the capabilities of the full WIEN2k package [22,23] by allowing for calculations in arbitrary noncollinear spin structures. The exchange-correlation potential was taken in the Generalized Gradient Approximation (GGA [24]). The charge density and potential were expanded in spherical harmonics within non-overlapping atomic spheres of radius R_{MT} and in plane waves in the remaining region of the unit cell. The sphere radius varied slightly depending on the structure and was chosen to be as large as possible in each system (while remaining constant within a single study). Typical R_{MT} values for atoms were: Fe: 2.34 a.u.; Al: 2.15 a.u.; B: 2.08 a.u.; Ga: 2.27 a.u.; V: 2.32 a.u.; Mn: 2.31 a.u. The decomposition of wave functions for valence electrons within atomic spheres was limited to $l_{\text{max}} = 12$, and they were calculated in a potential expanded in spherical harmonics up to $l = 6$. The wave functions in the interstitial region were expanded in plane waves with the cutoff vector K_{max} determined by the relation $R_{\text{MT}} \times K_{\text{max}} = 5.45$. The charge density was expanded in Fourier series up to $G_{\text{max}} = 20$. The grid of 4913 k -points ($17 \times 17 \times 17$) was chosen in the irreducible part of the Brillouin zone. We used the ‘FULL’ noncollinear magnetism mode, which includes off-diagonal elements in the potential matrix and accounts for noncollinearity within ‘muffin-tin’ spheres. The lattice parameter (equilibrium value) was determined based on the condition of the minimum total energy per unit cell. It was assumed that the unit cell was cubic. If necessary, the relaxation of interatomic distances within the unit cell was carried out until the forces acting on the atoms equated to zero using the WIEN2k program (a system with such an unit cell will be referred to as the relaxed system).

3. Results and Discussions

Quantum-mechanical calculations of the electronic structure of Fe-Al-based systems at various values and directions of the Spin Spiral Wave (SSW) propagation q -vector are of particular interest. The directions of the SSW vector are indicated in square brackets $[\zeta\zeta\zeta]$. The value of the SSW vector can vary from 0 to $2\pi/a$. Hereinafter, the state of the studied system with the SSW vector value of $q = 0$ will correspond to the ferromagnetic (FM) state, and the corresponding total energy of the unit cell, divided by the total number of atoms (16), is denoted by E_{FM} . The total energy at $q = 0.5 \times \pi/a$ (where a is the *bcc* lattice parameter) is denoted as E_{SSW} . At this value of the SSW vector, the minimum total energy of the unit cell is most often observed (e.g., Figure 2). In the context of the WIENncm program, the spin spiral

structure is a sophisticated form of noncollinear magnetic order in which magnetic moments continuously change from site to site (rotate) as one moves through successive unit cells. Unlike planar ISDWs, the spin spiral structure in WIENncm is inherently three-dimensional, allowing the magnetic moments to rotate in space without being confined to a fixed plane. This rotation occurs without any change in the magnitude of the magnetic moments, maintaining a constant amplitude throughout the system. In terms of the angles between Fe atoms in adjacent planes along the $[\zeta\zeta\zeta]$ direction, $q = 0.5 \times \pi/a$ means that from plane to plane, the spin direction is rotated by 90° . In other words, the wavelength of the SSW is $4a$. At $q = \pi/a$, the system exhibits an antiferromagnetic (AFM) state with oppositely directed magnetic moments in neighboring unit cells (the corresponding energy is E_{AFM}). Results of calculations for vectors with $q > \pi/a$ are not provided, as they merely indicate a change in the spiral chirality (becoming clockwise), and for energy values the ratio holds $E(\pi/a + q) = E(\pi/a - q)$.

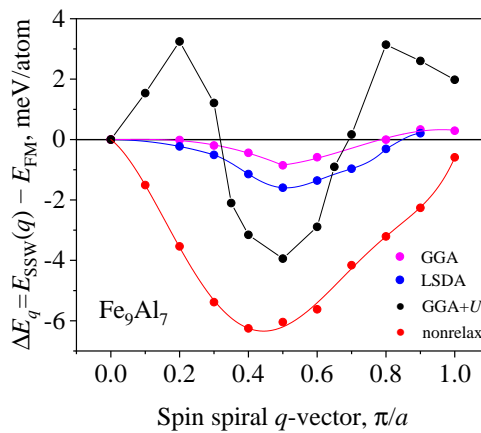


Figure 2. Dependence of the energy difference between SSW and FM states of the Fe_9Al_7 unit cell on the value of the SSW vector (in the crystallographic direction $[001]$) for various exchange-correlation potentials.

In Figure 2, for the q -vector direction $[001]$, the results of calculations of the difference (ΔE_q) in the total energies of unit cells (Figure 1) in the SSW and FM states for various values of the SSW vectors are presented. The calculations were performed using three different exchange-correlation potentials (GGA, LSDA, GGA+ U ($U_{\text{eff}} = 0.6$ eV)). The choice of this U_{eff} value was related to the necessity of comparing calculation results with measured values of the hyperfine magnetic field from Mössbauer spectroscopy data. It is clearly seen that, according to the obtained calculations, the ground state of the system is not ferromagnetic but represents spin spiral magnetic structure with the value of the SSW vector equal to $q = 0.5 \times \pi/a$. The qualitative nature of the obtained results remains unchanged across different potentials (and the value of U_{eff}). However, since the GGA method is the most commonly used and accepted for Fe-based systems [25–27], we will use only this method in further calculations. Additionally, calculations without accounting for the relaxation of interatomic distances (shown as red dots for nonrelaxed structures in Figure 2) are presented. Although the position of the energy minimum shifts to the value $q = 0.4 \times \pi/a$, we consider this to be an insignificant change, as it was never observed again in our calculations for binary Fe_9Al_7 supercells (including Figure 3). Thus, considering the relaxation of interatomic distances in the unit cell for the binary Fe-Al system affects the final conclusion only quantitatively, namely, it reduces the energy difference ΔE_q .

We next investigated other directions for SSW propagation. In Figure 3, the dependence of

the energy difference ΔE_q on the value of the SSW vector for the three main directions in the *bcc* system [111], [110], and [001] is presented, similar to Figure 2. According to our calculations, the spin spiral magnetic structure in the binary Fe_9Al_7 system can exist in all three specified directions. However, under otherwise equal conditions, the [111] direction appears to be the most energetically favorable and is therefore more likely to be realized in actual systems. This is confirmed by the neutron diffraction results [7,8].

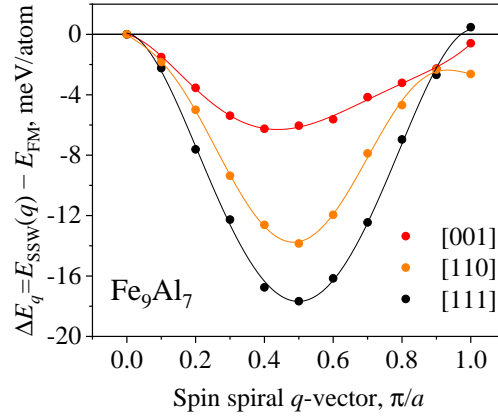


Figure 3. Dependence of the energy difference between SSW and FM states of the Fe_9Al_7 unit cell on the value of the SSW vector in the crystallographic directions [001], [110], and [111].

Of particular interest is the investigation of noncollinear magnetic structures in Fe-Al systems at various aluminum concentrations. For this purpose, spin spiral structure calculations were carried out for unit cells Fe_8Al_8 (50 at.% Al), Fe_9Al_7 (43.75 at.% Al, Figure 1), $\text{Fe}_{10}\text{Al}_6$ (37.5 at.% Al), $\text{Fe}_{11}\text{Al}_5$ (31.25 at.% Al), and $\text{Fe}_{12}\text{Al}_4$ (25 at.% Al). To understand the factors leading to the breakdown of the spin spiral magnetic state, calculations were performed at different lattice parameter values. It is known that with an increase in the lattice parameter of Fe-*sp* systems (and, consequently, the distance between Fe atoms), the total magnetic moment of the unit cell grows (a linear dependence is also confirmed in our calculations) [28–31]. Thus, the abscissa in Figure 4 represents the average magnetic moment, calculated as the total magnetic moment of the unit cell divided by the number of iron atoms. The negative region on the graph corresponds to the spin spiral state, indicating that only the Fe_9Al_7 structure retains the spin spiral state across nearly the full range of magnetic moments (lattice parameter) values and transitions to the ferromagnetic state only above $\approx 2 \mu_B/\text{Fe}$ atom.

It should be noted here that the value of the average magnetic moment, where the spin spiral magnetic state is most favorable, is approximately $1 \mu_B/\text{Fe}$ atom. For Fe_8Al_8 and $\text{Fe}_{10}\text{Al}_6$, there are isolated solutions (each point on the graph represents, in essence, the solution of the quantum-mechanical problem using density functional theory), at which the spin spiral structure is energetically favorable, but no stable range can be identified. This contrasts with high-iron-concentration systems: $\text{Fe}_{11}\text{Al}_5$ and $\text{Fe}_{12}\text{Al}_4$, where ferromagnetic ordering is stably realized. Only through significant compression of the $\text{Fe}_{11}\text{Al}_5$ unit cell (thus reducing the total magnetic moment to the minimum at which the quantum-mechanical solution can be obtained) can the spin spiral state be achieved in such a system. Notably, for the [001] direction, the SSW was not observed in any structures except Fe_9Al_7 .

The reason for such diverse results for different concentrations of at.% Al is related to the unique structure of Fe_9Al_7 , characterized by an “ Fe_9 cube” surrounded by *sp*-elements (Al).

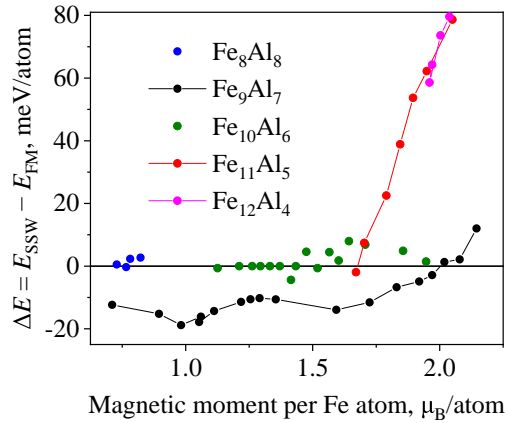


Figure 4. Dependence of the energy difference between SSW and FM states on the average magnetic moment for various 16-atom unit cells.

These “cubes” are not directly connected by exchange interactions through other iron atoms (for example, those at the crystallographic position (0;0;0) in Figure 1). Instead, any “intercube” interactions occur via superexchange mediated by aluminum atoms. This makes the magnetic moments within the “cubes” more susceptible to rotation, thereby contributing to the formation of spiral magnetic structures in various crystallographic directions (such as [001], [110], or [111]). The influence of exchange interactions on noncollinear magnetic order is examined by deriving effective exchange interactions J_{ij} from ab initio calculations, as presented in [14]. These interactions are crucial for understanding the emergence of noncollinear magnetic orders, and their interplay is revealed in the context of varying lattice parameters through magnetic phase diagrams. These diagrams display different magnetic states, such as ferromagnetic, antiferromagnetic, and spiral ISDW order, as a function of the exchange interactions between nearest neighbors.

Conversely, such a “cube” is simply absent in the Fe_8Al_8 structure. However, additional calculations (Table 1) for the Fe_4Al_4 (50 at.% Al) structure (Figure 5) showed that besides the main ferromagnetic state, such a structure also has two other solutions: AFM – with alternating signs of magnetic moments of iron atoms [up, down, up, down]; SSW – with alternating directions of magnetic moments through zero [up, zero, down, zero]. Despite the fact that these AFM and SSW solutions are not energetically advantageous, their energy difference from the ferromagnetic solution does not exceed 0.01 eV per atom, which is less than $k_B T$ at room temperature. The calculated values of the local magnetic moments for the four iron atoms (m_i^{Fe} from left to right) for the three aforementioned types of magnetic ordering are presented in Table 1. The last column lists the total energy of the system, where the total energy of the unit cell with the ferromagnetic type of magnetic ordering is taken as the reference zero. In this calculation, we consider magnetic ordering type characterized by amplitude modulation of the magnetic moments, known as ISDW. In this configuration, the magnetic moments lie within a single plane, but their magnitudes vary periodically across the system. This results in a wave-like modulation where the magnetic moments remain collinear within the plane, while their magnitudes change, creating a periodic pattern.

Next, we investigate ternary alloys based on Fe-Al with small additives of boron or gallium. In contrast to Fe_9Al_7 , calculations for the Fe_9Al_6B unit cell (Figure 6) show that relaxing interatomic distances makes the spin spiral magnetic state less favorable compared to the FM state.

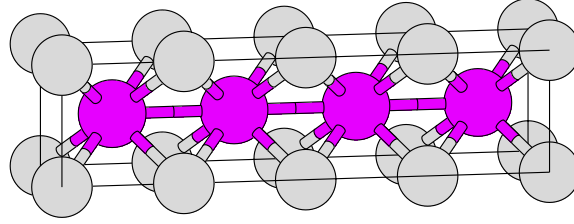


Figure 5. Unit cell of Fe_4Al_4 . Purple spheres correspond to iron atoms, gray spheres to aluminum atoms.

Table 1. Local magnetic moments of iron atoms in the Fe_4Al_4 structure.

| | $m_1^{\text{Fe}}, \mu_{\text{B}}$ | $m_2^{\text{Fe}}, \mu_{\text{B}}$ | $m_3^{\text{Fe}}, \mu_{\text{B}}$ | $m_4^{\text{Fe}}, \mu_{\text{B}}$ | $E, \text{meV/atom}$ |
|-----|-----------------------------------|-----------------------------------|-----------------------------------|-----------------------------------|----------------------|
| FM | 0.70 | 0.70 | 0.70 | 0.70 | 0 |
| AFM | 0.62 | -0.62 | 0.62 | -0.62 | 10 |
| SSW | 0.84 | 0 | -0.84 | 0 | 8 |

Figure 6 demonstrates that the nonrelaxed supercell favors the spin spiral magnetic state (red dots), whereas the relaxed supercell favors the ferromagnetic state (pink dots). This leads us to conclude that a potential mechanism for the breakdown of the spin spiral structure involves changes in the atomic positions in the unit cell (for example, the presence of defects, including substitutional impurities). The features described above are likely due to size differences between boron and aluminum atoms. Replacing Al with B significantly alters the distribution of forces acting on the atoms, requiring the atoms to adjust to their equilibrium positions, which ultimately disrupts the spin spiral structure. For comparison, the direction of spin spiral structure propagation [111] is also provided, which remains energetically more favorable for the ternary Fe-Al-B system.

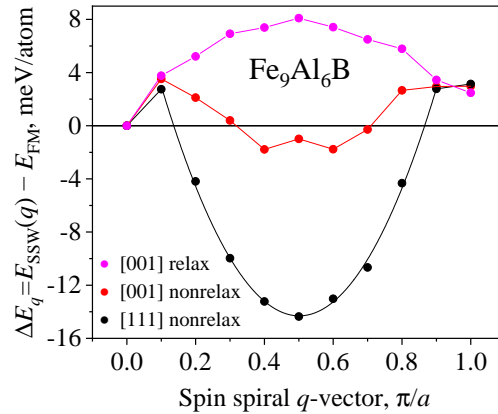


Figure 6. Dependence of the energy difference between SSW and FM states of the $\text{Fe}_9\text{Al}_6\text{B}$ unit cell on the value of the SSW vector in the crystallographic directions [001] and [111].

In the Fe_9Al_7 structure (see Figure 1), the boron atom can replace aluminum in only three nonequivalent positions: (0;0;0) (the case in Figure 6), (0;0;1/2), and (1/2;1/2;0). The results of spin spiral magnetic structure calculations in the [111] crystallographic direction for all three boron substitution positions in the relaxed unit cell are presented in Figure 7. It is observed

that, as in the [001] direction, the relaxation of atomic positions leads to the destabilization of the spin spiral structure when boron occupies the (0;0;0) and (0;0;1/2) sites. However, stable spin spiral structure is observed within the $\text{Fe}_9\text{Al}_6\text{B}$ supercell configuration when the boron atom is located at the (1/2;1/2;0) position, even under conditions of relaxed atomic positions within the unit cell. Thus, the calculation results indicate that specific conditions must be met for the stable existence of a spin spiral magnetic structure in the ternary Fe-Al-B system (where boron substitutes for aluminum): specific atomic site configurations within the unit cell and the orientation of SSW propagation relative to the substituted atom.

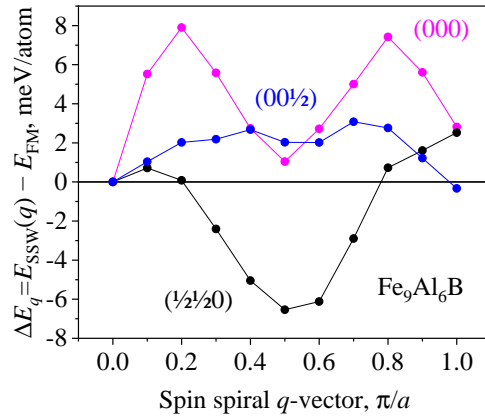


Figure 7. Dependence of the energy difference between SSW and FM states of the $\text{Fe}_9\text{Al}_6\text{B}$ unit cell on the value of the SSW vector for various substitutional atom positions.

An even more remarkable phenomenon is observed in the $\text{Fe}_9\text{Al}_6\text{Ga}$ system. On the curve corresponding to the nonrelaxed system (red curve in Figure 8), a local minimum is observed around the value $q = 0.1 \times \pi/a$. This extremum becomes fully visible after the relaxation of interatomic distances within the unit cell (pink curve in Figure 8). Thus, in the ternary Fe-Al system with small gallium additions, apart from the main mode (wavelength of the SSW is $4a$) in the [001] direction, the spin spiral structure with the wavelength $\approx 20a$ may be observed. Importantly, the wavelength of the SSW in the [111] direction remains independent of atomic positions, maintaining its status as the energetically most favorable direction (black curve in Figure 8).

A more detailed analysis of the SSW order along the [111] crystallographic direction for $\text{Fe}_9\text{Al}_6\text{B}$ and $\text{Fe}_9\text{Al}_6\text{Ga}$ nonrelaxed structures is presented in Figure 9 (compared to Fe_9Al_7). Figure 9a shows a dependence of the calculated energy difference between SSW and FM states on the average magnetic moment for ternary systems with all possible substitution atom positions. It is observed in each scenario, there is a range of lattice parameter values (Figure 9b) within which the SSW state is energetically more favorable than the FM state. Moreover, the behavior of the $\text{Fe}_9\text{Al}_6\text{Ga}$ system resembles more closely that of the binary Fe_9Al_7 than $\text{Fe}_9\text{Al}_6\text{B}$. For Fe_9Al_7 and $\text{Fe}_9\text{Al}_6\text{Ga}$, the energy difference between FM and SSW states is approximately 18 meV per atom, whereas for $\text{Fe}_9\text{Al}_6\text{B}$, it is about 5 meV per atom. One of the conclusions drawn from the analysis is that each of the considered systems has a minimum SSW state energy at an average magnetic moment value of $\approx 1 \mu_B/\text{Fe}$ atom (Figure 9a). As shown in Figure 9b, the value of the lattice parameter at the extremum (and the equilibrium lattice parameter value) differs for all systems, in contrast to the average magnetic moment (Figure 9a). From this, we conclude that the magnitude of the magnetic moment per iron atom, determined by exchange

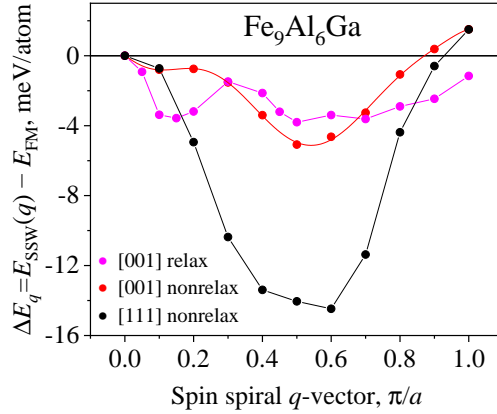


Figure 8. Dependence of the energy difference between SSW and FM states of the $\text{Fe}_9\text{Al}_6\text{Ga}$ unit cell on the value of the SSW vector in the crystallographic directions [001] and [111].

interactions, is essential for the existence of the SSW solution. It was hypothesized that the destabilization of the spin spiral structure would occur at the same magnetic moment value for all considered unit cells. However, our calculations do not confirm this hypothesis (Figure 9a).

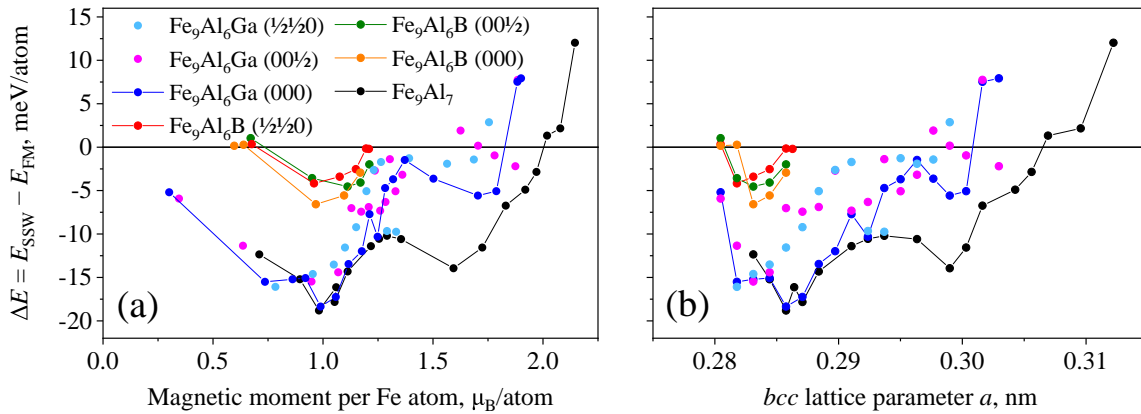


Figure 9. Dependence of the energy difference between SSW and FM states on (a) the average magnetic moment and (b) the lattice parameter for various 16-atom unit cells.

To investigate the influence of Al atoms on the existence of SSW, similar calculations were carried out for the supercells Fe_9Si_7 , Fe_9Ga_7 and Fe_9B_7 . Upon substituting all aluminum atoms with isoelectronic gallium atoms, the energy profile (Figure 10a) exhibits identical characteristics to that of Fe_9Al_7 . That is, according to our calculations, the spin spiral state is energetically favorable in Fe-Ga binary systems. Neutron diffraction experiments reported in [13] have demonstrated the presence of ISDW ordering in Fe_3Ga_4 . That finding agrees with our results. All the previous conclusions for Fe-Al are valid for this structure. Our calculation show that for the Fe_9Si_7 supercell (Figure 10b) the spin spiral state is energetically favorable in a very narrow range of lattice parameter values (from 0.278 nm to 0.281 nm). As well the energy profile exhibits significantly different behavior compared to Fe_9Al_7 and Fe_9Ga_7 (suggesting a potentially differing underlying mechanism) and is similar to that observed in the systems discussed in [15, 16]. The value of the SSW vector at the energy minimum is approximately $q = 0.1 \times \pi/a$, which corresponds to an SSW-length of $\approx 20a$. For the Fe_9B_7 structure, no consistent trend of the total energy on the SSW vector was detected. According to our calculations, the ferromagnetic

state remains energetically favorable for this case, and a SSW state was not identified.

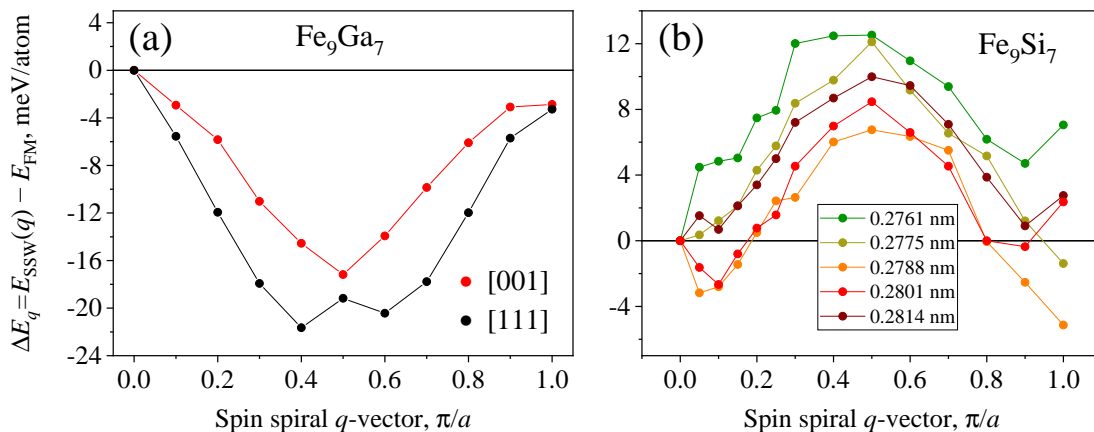


Figure 10. Dependence of the energy difference between SSW and FM states of the unit cells of binary systems (a) Fe_9Ga_7 and (b) Fe_9Si_7 on the value of the SSW vector.

We compare the results of our calculations regarding the magnitude of the magnetic moment that allows the stability of SSW with data from comprehensive magnetometric and Mössbauer experimental studies [19, 20, 32]. The analysis of the magnetic state of ordered alloys $\text{Fe}_{65}\text{Al}_{35}$, $\text{Fe}_{65}\text{Al}_{30}\text{Ga}_5$, and $\text{Fe}_{65}\text{Al}_{30}\text{B}_5$ performed in these works (the Mössbauer spectra are presented in Figure 11a) led to the conclusion of magnetic phase separation in the samples. Two phases were identified: the first is ferromagnetic, and the second relates to incommensurate long-period structures of the SSW or ISDW type and does not contribute to the resulting magnetization. Note that the shaded area of the Mössbauer spectrum corresponding to the second phase has a similar appearance for all the alloys and is defined over the same interval of effective HMF.

During mathematical processing, it is possible to represent this component of the spectra in the form of either SSW or ISDW with equal quality, within experimental error. The calculation of the experimental spectra was performed for both variants. However, for this particular system of alloys and at the current stage of understanding the dynamics of such spin structures, SSW and ISDW are not clearly differentiated in the Mössbauer spectra. Since the theoretical calculations in this work were carried out for a magnetic structure of the SSW type, it was natural to perform an analysis of the Mössbauer spectra in which the partial component of the second non-ferromagnetic phase is formalized in the form of SSW [33].

The HMF distributions $p(B_{\text{hf}})$ corresponding to this magnetic structure are presented in Figure 11b, where the average HMF values $\langle B_{\text{hf}} \rangle$ are also indicated. This magnetic structure corresponds to one of the types we studied (Figure 5, Table 1), which is characterized by modulation not only of the direction of the magnetic moment but also of the amplitude. Such ordering of the magnetic moment from one unit cell to another, accompanied by variations in both direction and amplitude, can be considered the most general case of a static noncollinear long-period magnetic structure. In this context, modulation of only the amplitude (the case of collinear ordering) or only the direction can be regarded as special cases of such magnetic order.

The value of the average HMF $\langle B_{\text{hf}} \rangle$, obtained from the HMF distribution within the so-called “model-free” processing of the non-ferromagnetic component of the spectra [34], and in representing this component in the form of SSW is the same and amounts to approximately 9.1 ± 0.2 T. From this, one can formally make an approximate estimate of the average value

of the magnetic moment (per Fe atom) $\langle m^{\text{Fe}} \rangle$ for the non-ferromagnetic SSW phase. The proportionality constant between the HMF values B_{hf} and the magnetic moment $\langle m^{\text{Fe}} \rangle$ used for this estimate (for single-phase Fe–Al, Fe–Si, and Fe–Sn alloys in the ground state) ranges from 11.0 to 14.0 T/ μ_{B} [35,36]. Thus, the average value $\langle m^{\text{Fe}} \rangle$ of the magnetic moments forming the static SSW in the considered alloys, equivalent to the observed average HMF $\langle B_{\text{hf}} \rangle$, turns out to be $m^{\text{Fe}} \approx 0.7 \div 0.8 \mu_{\text{B}}$.

Considering that the value of the average magnetic moment obtained from the experiment is roughly estimated, the agreement between the theoretical value and the experimental estimate of the average magnetic moment should be recognized as satisfactory. Additionally, the numerical predictions of the DFT method do not always correspond with high accuracy to the observed values of magnetic moments and parameters of hyperfine interactions. Therefore, despite these discrepancies, the overall agreement between theory and experiment remains acceptable. At the same time, the authors believe that the main point in this analysis is not the precision in reproducing the absolute value of the average magnetic moment, but the correspondence and consistency across all the systems considered.

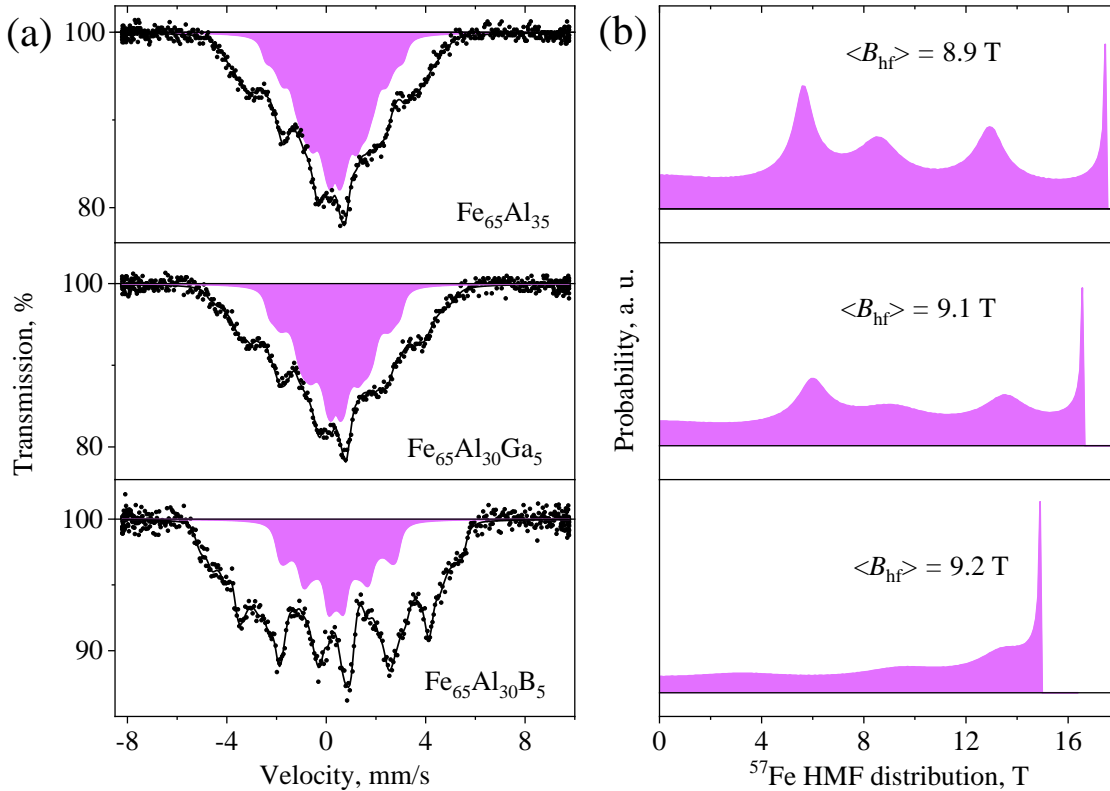


Figure 11. (a) Mössbauer spectra of ordered $\text{Fe}_{65}\text{Al}_{35}$, $\text{Fe}_{65}\text{Al}_{30}\text{Ga}_5$, and $\text{Fe}_{65}\text{Al}_{30}\text{B}_5$ alloys; the shaded partial component of the spectra corresponds to ^{57}Fe nuclei associated with SSW-type magnetic ordering, with the distribution of the HMF shown in (b).

4. Summary

In this work, the magnetic structure of binary Fe–Al and ternary $\text{Fe}_9\text{Al}_6\text{B}$, $\text{Fe}_9\text{Al}_6\text{Ga}$ systems was studied within Density Functional Theory. It was shown that the ferromagnetic state is found to be energetically unfavorable, and in most cases, the spin spiral wave state is realized. The use of different exchange-correlation potentials yields a similar qualitative picture of the total energy

dependence on the value of the spin spiral wave q -vector for all the systems, with the generalized gradient approximation method giving the most consistency with observed phenomena.

In binary Fe-Al systems, the spin spiral structure was observed only in the Fe_9Al_7 unit cell (43.75 at.% Al). For other aluminum concentrations in the 16-atom unit cell, ferromagnetic state is realized according to our calculations. Calculations also showed that all three directions of the spin spiral wave vector: [001], [110], and [111] can exist in the Fe-Al system. However, the most energetically favorable direction is [111], which is observed in neutron diffraction experiments.

The position and type of sp -elements within the unit cell affect the energy difference between the spin spiral and ferromagnetic states. Whether one of these states is equilibrium depends on both the atomic positions within the unit cell and the type of atom at the position (Al or B or Ga). Nevertheless, calculations showed that in ternary systems $\text{Fe}_9\text{Al}_6\text{B}$ and $\text{Fe}_9\text{Al}_6\text{Ga}$, the ground state is also characterized by the spin spiral wave with the [111] direction of q -vector.

For all systems under consideration, the spin spiral state is energetically most favorable at such a lattice parameter value where the average magnetic moment is $\approx 1 \mu_{\text{B}}/\text{Fe}$ atom, regardless of the substitutional atom's position.

Comparative analysis of Fe_9Al_7 and Fe_9Ga_7 , Fe_9Si_7 , Fe_9B_7 structures demonstrated that all obtained results are not coincidental and depend of the electronic structure on the sp -element. Isoelectronic atoms of Al and Ga exhibit similar behavior, forming a stable spin spiral structure in alloy with iron, whereas Fe-Si and Fe-B alloys exhibit completely different magnetic properties.

The approximate value of the average magnetic moment of iron atoms involved in the spin spiral structure, $m^{\text{Fe}} \approx 0.7 \div 0.8 \mu_{\text{B}}$, based on the analysis of Mössbauer spectroscopy data, is in satisfactory agreement with the theoretical calculation result.

References

1. Arrott A., Sato H., *Physical Review* **114**, 1420 (1959).
2. Danan H., Gengnagel H., *Journal of Applied Physics* **39**, 678 (1968).
3. Cable J. V., David L., Parra R., *Physical Review B: Solid State* **16**, 1132 (1977).
4. Shukla P., Wortis M., *Physical Review B: Condensed Matter* **21**, 159 (1980).
5. Shull R. D., Okamoto H., Beck P. A., *Solid State Communications* **20**, 863 (1976).
6. Bao W., Raymond S., Shapiro S. M., Motoya K., Fåk B., Erwin R. W., *Physical Review Letters* **82**, 4711 (1999).
7. Noakes D. R., Adroja D. T., Rainford B. D., Bud'ko S. L., *Physical Review Letters* **91**, 217201 (2003).
8. Noakes D. R., Rainford B. D., Adroja D. T., Kockelmann W., Bud'ko S. L., Canfield P. C., *Journal of Applied Physics* **95**, 6574 (2004).
9. Bogner J., Ziebeck K. R. A., Baron A. Q. R., Schuster K., *Physical Review B* **58**, 14922 (1998).
10. Kulikov N. I., Postnikov A. V., Borstel G., Braun J., *Physical Review B* **59**, 6824 (1999).
11. Kaptás D., Sváb E., Somogyvári Z., André G., Kiss L. F., Balogh J., Bujdosó L., Kemény T., Vincze I., *Physical Review B* **73**, 012401 (2006).

12. Wilfong B., Sharma V., Naphyetal J., *Journal of Alloys and Compounds* **894**, 162421 (2022).
13. Wu Y., Ning Z., Cao H., Cao G., Benavides K. A., Karna S., McCandless G. T., Jin R., Chan J. Y., Shelton W. A., DiTusa J. F., *Scientific Reports* **8**, 5225 (2018).
14. Tanveer M., Ruiz-Díaz P., Pastor G. M., *Physical Review B* **94**, 094403 (2016).
15. Grytsiuk S., Romhányi N., Gondolf K., Bouaziz J., Bouhassoune M., Schena T., Meyerheim H. L., Szunyogh L., Blügel S., Mokrousov Y., *Physical Review B* **100**, 214406 (2019).
16. Loh G. C., Gan C. K., *AIP Advances* **7**, 055704 (2017).
17. Abdullin A. F., Voronina E. V., Dobysheva L. V., *Uchenye Zapiski Kazanskogo Universiteta. Seriya Fiziko-Matematicheskie Nauki* **162**, 455 (2020), [in Russian].
18. Voronina E. V., Al'Saedi A. K., Ivanova A. G., Arzhnikov A. K., Dulov E. N., *Physica Status Solidi A* **120**, 1213 (2019).
19. Voronina E. V., Arzhnikov A. K., Chumakov A. I., Chistyakova N. I., Ivanova A. G., Pyataev A. V., Korolev A. V., *Advances in Condensed Matter Physics* **2018**, 5781873 (2018).
20. Voronina E. V., Ivanova A. G., Arzhnikov A. K., Chumakov A. I., Chistyakova N. I., Pyataev A. V., Korolev A. V., *Physics of the Solid State* **60**, 730 (2018).
21. Laskowski R., K. M. G., Blaha P., Schwarz K., *Physical Review B* **69**, 140408 (2004).
22. Blaha P., Schwarz K., Madsen G. K. H., Kvasnicka D., Luitz J., Laskowski R., Tran F., Marks L. D., *WIEN2k, An Augmented Plane Wave + Local Orbitals Program for Calculating Crystal Properties* (2018).
23. Blaha P., Schwarz K., Tran F., Laskowski R., Madsen G. K. H., Marks L. D., *The Journal of Chemical Physics* **152**, 074101 (2020).
24. Perdew J. P., Burke K., Ernzerhof M., *Physical Review Letters* **77**, 3865 (1996).
25. Comtesse D., Herper H. C., Hucht A., Entel P., *The European Physical Journal B* **85**, 1 (2012).
26. Matyunina M., Zagrebin M., Sokolovskiy V., Buchelnikov V., *EPJ Web of Conferences* **185**, 04013 (2018).
27. Hou Z., Takagiwa Y., Shinohara Y., Xu Y., Tsuda K., *Journal of Physics: Condensed Matter* **33**, 195501 (2021).
28. Andersen O. K., Madsen J., Poulsen U. K., Jepsen O., Kollar J., *Physica B+C* **86**, 249 (1977).
29. Kübler J., *Physics Letters A* **81**, 81 (1981).
30. Shiga M., *IEEE Translation Journal on Magnetism in Japan* **6**, 1039 (1991).
31. Arzhnikov A. K., Dobysheva L. V., Brauers F., *Physics of the Solid State* **42**, 89 (2000).
32. Voronina E. V., Abdullin A. F., Ivanova A. G., Dobysheva L. V., Korolev A. V., Arzhnikov A. K., *Journal of Experimental and Theoretical Physics* **136**, 89 (2023).

DFT study of magnetic order in Fe-Al-based ternary alloys

33. Matsnev M. E., Rusakov V. S., *AIP Conference Proceedings* **1489**, 178 (2012).
34. Ageev A. L., Voronina E. V., *Journal of Nuclear Instruments and Methods B* **108**, 417 (1996).
35. Yelsukov E. P., Konygin G. N., Voronina E. V., *Izvestiya Rossiiskoi Akademii Nauk. Seriya Fizicheskaya* **56**, 119 (1992), [in Russian].
36. Yelsukov E. P., Voronina E. V., Konygin G. N., Barinov V. A., Godovikov S. K., Dorofeev G. A., Zagainov A. V., *Journal of Magnetism and Magnetic Materials* **166**, 334 (1997).